3. Modulation of the Anomalous and Galactic Components of Cosmic Ray H and He as described by a Full-Drift Two-Dimensional Acceleration Model

C.D. Steenberg, H. Moraal and F.B. McDonald

3.1. Introduction

The deep-space missions of Pioneers 10 and 11 and Voyagers 1 and 2 have contributed greatly to our understanding of the modulation of galactic and anomalous cosmic rays in the outer heliosphere. The Space Research Unit of the Potchefstroom University has focused primarily on developing numerical models to solve the cosmic ray transport equation, as discussed at length by Reinecke *et al.* (1993). The availability of new outer heliospheric observations, made during a $qA > 0$ solar cycle, provides new opportunities to study the modulation of cosmic rays in the heliosphere.

Our present studies are a continuation of the work by McDonald *et al.* (1992), Reinecke *et al.* (1993) and Reinecke *et al.* (1996), that applied a stationary two-dimensional modulation model (excluding shock acceleration) to the 1977/78 and 1987 GCR Proton, GCR and ACR He, and ACR O, as well as of Steenkamp and Moraal (1993), Steenkamp (1995), Steenberg and Moraal (1996), and Steenberg and Moraal (1997) that applied a time-dependent two-dimensional shock acceleration model (Steenkamp, 1995) to these sets of observations. We now apply the latter model to H and He observations made during the first and second Ulysses polar passes in 1994/95, as well as recent 1996 observations, fitting both the ACR and GCR components simultaneously, a method which places new limits on the scattering parameters in the model.

3.2. The Model

Steenkamp (1995) developed a numerical code that solves the time-dependent cosmic ray transport equation

$$\frac{\partial f}{\partial t} = \nabla \cdot (\mathbf{K} \cdot \nabla f - f\boldsymbol{V}) \frac{1}{3p^2} (\nabla \cdot \boldsymbol{V}) \frac{\partial}{\partial p}(p^3 f) + Q, \qquad (1)$$

in a two-dimensional axisymmetric heliosphere for the omnidirectional distribution function $f(r, \theta, P)$, as a function of radial distance, r, polar angle, θ, and rigidity

$P = pc/q$, with p the particle momentum, c the speed of light and q its ionic charge. In our calculations we placed the modulation boundary at $r_b = 120$ AU, and a compression ratio $s = 4$ solar wind termination shock (SWTS) at $r_s = 90$ AU. We used a nonlinear radial grid with 100 intervals inside the SWTS and 40 from the SWTS to the outer boundary, with the smallest spacing of 0.04 AU around the SWTS. At the boundary the intensity was set equal to the assumed local interstellar spectrum,

$$j_b = P^2 f_b = N\beta/(T + 0.5E_0)^{2.6} \text{ particles/(m}^2\text{sr s MeV/nuc)} \quad (2)$$

for both the GCR H and He calculations, where P is particle rigidity and T is kinetic energy per nucleon in units of MeV/nuc. The factor N is a normalization constant, β denotes the particle speed relative to that of light, and E_0 is the rest mass energy of a proton. For the ACR component, particles were injected at the SWTS using the source function

$$Q(r, P) = Q_0 \delta(r - r_s)\delta(P - P_i), \quad (3)$$

with an injection rigidity of $P_i = pc/q = 0.1$ GV ($T_i \approx 5$ MeV for protons, $T_i \approx 0.3$ MeV/nuc for He^+, $T_i \approx 1.25$ MeV/nuc for He^{++}). The value of Q_0 is determined by the ionization efficiency of interstellar neutrals and the injection efficiency of thermal particles at the shock, and was taken to be a free parameter. At the SWTS the radial solar wind speed, V, discontinuously drops by the compression ratio, $s = 4$, from $V = V_0 l(\theta)$ to $V = V_0 l(\theta)(r_s/r)^2/s$ km/s outside the shock, with $V_0 = 400$ km/s and $l(\theta) = 1.5 + 0.5\cos(2\theta)$ increasing from 1 in the ecliptic ($\theta = \pi/2$) to 2 over the poles ($\theta = 0, \pi$)), as shown in panel A of Figure 11. A linear latitudinal grid, with 30 intervals of 3° each, running from the pole ($\theta = 0°$) to the ecliptic ($\theta = \pi/2$) was used, assuming latitudinal symmetry around the solar poles and the ecliptic, i.e. $\partial f/\partial\theta = 0$ for $\theta = 0, \pi/2$. A rigidity grid from $P = 0.09$ to 20 GV, divided logarithmically in 264 intervals, was used, with the boundary conditions that the intensity is zero at the lowest rigidity, and that no modulation takes place at the highest. All solutions are time-asymptotic for a total model time of 2.6 years.

Also included are the effects of particle drifts in an unmodified Parker spiral field, with a field strength of $B = 5$ nT at Earth and a simulated neutral sheet with a tilt angle of 10°. These magnetic field parameters were not varied between the different observation periods, because drift effects only had a minimal effect on the model calculations due to the large magnitude of the diffusion coefficients used.

3.3. Data Base

We apply the model described above to H and He observations made during the $qA > 0$ drift cycle for the periods of the first and second Ulysses polar passes (1994/178–309 and 1995/170–273 respectively) as well as during 1996. Table III shows the sources of the data, as well as the observation periods, if different from

Table III

Summary of data collection periods and sources. The abbreviation ISSI indicates that the data are from the source mentioned in Section 2, while GSFC indicates data from Goddard Space Flight Center experiments. The observation periods are 1994/178-309 and 1995/170-273, unless otherwise indicated by the numbers in brackets for a particular year.

	H			He		
Spacecraft	1994	1995	1996	1994	1995	1996
IMP8			GSFC (1-131)			GSFC (1-131)
V1	ISSI	ISSI	GSFC (1-153)	ISSI	ISSI	GSFC (1-153)
V2	ISSI	ISSI	GSFC (1-32)	ISSI	ISSI	GSFC (1-32)
P10	GSFC	GSFC (169-247)	GSFC (1-138)	ISSI	ISSI	GSFC (1-138)

those mentioned above. In this table, sets marked "ISSI" are more fully described in Section 2, while those marked "GSFC" are from Goddard Space Flight Center experiments. These observations are illustrated in Figure 3.3, which serves as a prototype for presenting the observations in this contribution.

The observed 1996 H and He spectra cover a broad energy band from 3–300 MeV for H and 3–500 MeV/nuc for He, clearly showing both the ACR and GCR components of these species. Furthermore, the spectral peak energies of both these components are included in these energy ranges, enabling us to restrict our parameter choice to a very narrow range of values. In contrast, the 1994 and 1995 data did not include the GCR component.

3.4. Model Calculations

We now present results of our first attempt to model the ACR and GCR observations presented above, using a time-dependent acceleration/re-acceleration and modulation model. Following the success in fitting 1987 ACR He and O spectra by Steenberg and Moraal (1997), we used the simplest possible spatial diffusion model, namely spatially independent radial and latitudinal diffusion coefficients, $\kappa_{rr} = \kappa_{rr0}\beta P$ and $\kappa_{\theta\theta} = \kappa_{\theta\theta 0}\beta P$, illustrated in Figure 7 as a first step. The differences in the curves shown are accounted for by the different values of β, at the same rigidity, which are determined by the particle mass number to charge ratio, A/Z.

According to Le Roux *et al.* (1996), the magnitude of κ_{rr} at the shock determines the curvature cutoff of the spectra at the shock. Using our set of parameters, the form of these shock spectra turns out to be one of the important modulation parameters that determines the characteristics of modulated ACR spectra. Thus, our choice of the magnitude of κ_{rr} at the shock was restricted by the form of the shock spectra, that, along with other modulation parameters, determines the form of the modulated ACR spectra. The model results for ACR and GCR H and He are discussed in the next section.

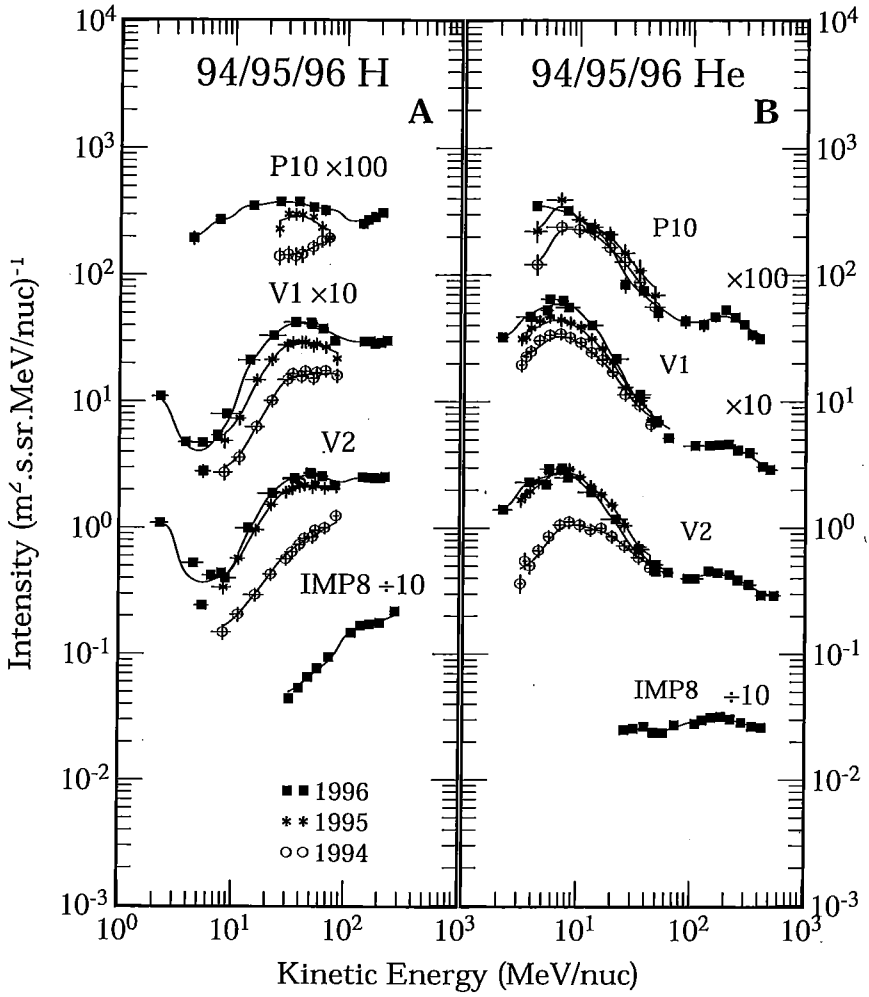

Figure 6. Observed spectral intensities during 1994, 1995 and 1996 for H (panel A) and He (panel B). In this Figure the data sets from different spacecraft are separated by factors of ten to aid visualization, while a solid line was drawn through every set of points to guide the eye.

3.4.1. *Protons*

ACR and GCR H spectra were calculated for each spacecraft position. These two calculated spectra were added to give the total calculated H intensity.

Figure 8 shows fits to the 1994, 1995 and 1996 H spectra, obtained using the parameters as summarized in Table IV. Note that the values of N in this table are such that the GCR input spectrum in (2) is about three times lower than the standard value, used by, e.g., Steenberg and Moraal (1996). This was needed because of the large magnitude of κ_{rr} (required to fit the ACR spectra). Careful comparison of

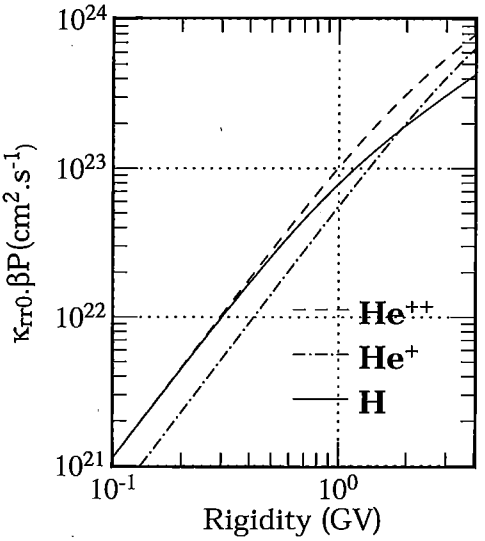

Figure 7. Spatially independent radial diffusion coefficients used to fit the observations as a function of rigidity. The different forms are due to the species dependence of β at a given rigidity.

Table IV

Summary of the parameters used to fit the spectra observations in 1994, 1995, and 1996. The diffusion coefficients are in units of cm^2/s ($\times 10^{23}$), Q_0 in particles/(m^2 s) ($\times 10^{-23}$), while N is in particles $(MeV/nuc)^{1.6}/(m^2\ s\ sr)$

	H				He				
	κ_{rr0}	$\kappa_{\theta\theta 0}$	Q_0	N	κ_{rr0}	$\kappa_{\theta\theta 0}$	Q_0 (He^+)	Q_0 (He^{++})	N
1994	1.08	1.08	3.71	3.82	2.16	2.16	4.74	4.74	0.319
1995	1.08	1.08	7.41	3.82	2.16	2.16	9.19	4.74	0.319
1996	1.08	1.08	7.41	3.82	2.16	2.16	9.19	4.74	0.319

the calculated and observed spectra shows that the calculated ACR gradients are somewhat larger than the observed ones.

To evaluate the diffusion coefficients used in this study, we first note that for $r \gg 1$ AU in a Parker spiral magnetic field, $\kappa_\perp \approx \kappa_{rr} = 1.08 \times 10^{23} \beta P$ cm^2/s, which is ≈ 3.9 times the value of $\kappa_\perp = 3.6 \times 10^{22} \beta P$ used by Steenberg and Moraal (1997) to fit the 1997 H observations.

Table V shows the energies at which the maximum ACR H contribution to the total intensity occurs for the calculated spectra. For 1 AU these maximum contributions of about 15% occur at 5.3 MeV, while they occur at 23 MeV for all the spacecraft in the outer heliosphere. The relative size of the ACR contribution increases toward the outer heliosphere, as well as from 1994 to 1996, with a maximum calculated contribution of 89% at Voyager 1 in 1996.

Figure 9 shows radial intensity profiles for the ACR component. Panel A clearly

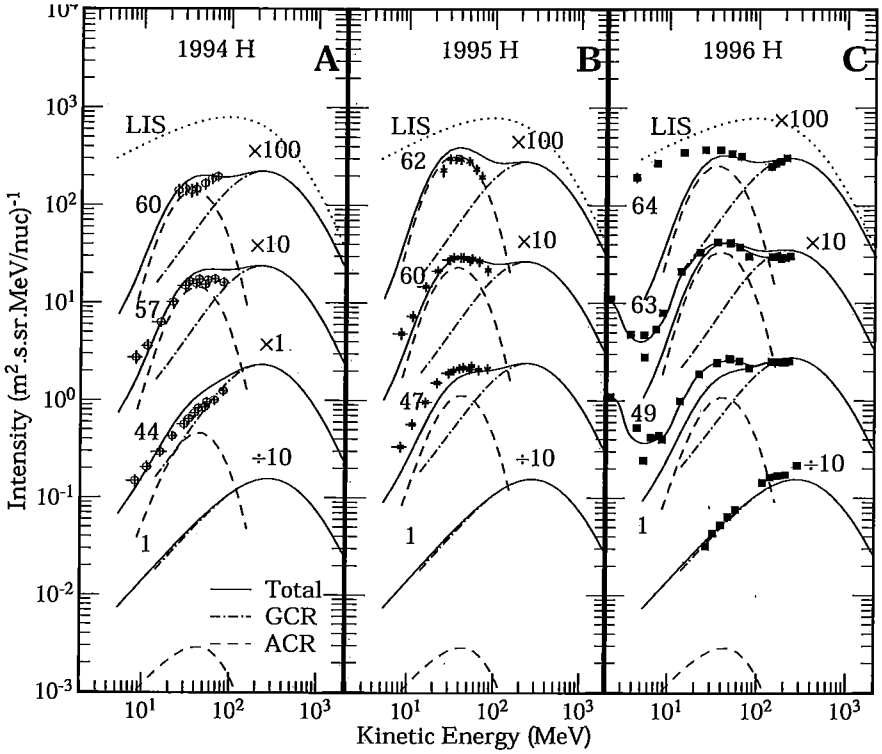

Figure 8. Model fits to the 1994/5/6 H observations in the same format as the observations presented in Figure 3.3, showing the modulated ACR and GCR components at the spacecraft positions as indicated by the number to the left of each data set. The total modulated spectrum was calculated as the sum of the ACR and GCR components.

Table V

Kinetic energies (MeV/nuc) at which the ACR H contribution to the total H intensity is largest. The percentage contribution at this energy is shown in brackets.

	IMP8	V2	V1	P10
1994	5.3 (15%)	23 (59%)	23 (83%)	23 (85%)
1995	5.3 (15%)	23 (69%)	23 (84%)	23 (88%)
1996	5.3 (15%)	23 (73%)	23 (89%)	23 (88%)

demonstrates the "skin depth" effect for 10 MeV particles: a large radial gradient for $r > 60$ AU, while the gradient for $r < 60$ AU is largely, if not totally, governed by the adiabatic limit of modulation. In the adiabatic limit, the particle intensities are independent of radial distance. "Skin depth" effect is used somewhat analogous to a similar concept for radiation entering an object, where the skin depth into the object is the distance at which the intensity of the radiation reaches a value

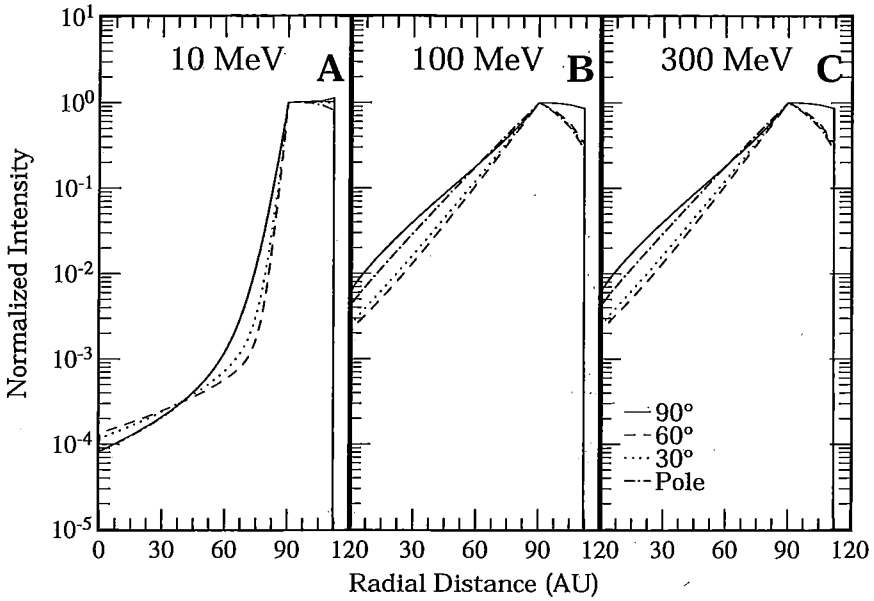

Figure 9. Radial intensity profiles for ACR H for four different polar angles, normalized at the SWTS intensity. Due to the same modulation parameters for all three periods, these profiles are identical for 1994, 1995, and 1996 ACR H. These profiles are also identical to those calculated for ACR He^{+} at 2.5, 25, and 75 MeV/nuc and at 5, 50, and 150 MeV/nuc for ACR He^{++}.

of $1/e$ of the intensity outside the object. The 100 and 300 MeV radial profiles in panels B and C of this figure, respectively, are similar and show the intensity, j, increasing approximately proportional to radial distance, r, with the 300 MeV intensities having a slightly larger gradient. The latitudinal dependence of the solar wind is largely responsible for the different profiles seen at higher latitudes. This is also illustrated by the latitudinal intensity profiles in Figure 11 which show a positive (small negative) latitudinal gradient in the outer (inner) heliosphere.

3.4.2. *Helium*

Following the method used in the previous paragraph for protons, we also calculated fits to the ACR and GCR He observations for the three observation periods. Using the same modulation parameters discussed in the previous paragraph, we found that the sum of a singly charged ACR component and the GCR component was unable to explain the observed ACR spectral peak width. We therefore included a doubly charged ACR He^{++} component (as described by Jokipii (1996) and Mewaldt *et al.* (1996b)) in our calculations and used a larger value for κ_{rr}, as indicated in Table IV. We note that for $r \gg 1$ AU in a Parker spiral magnetic field, $\kappa_{\perp} \approx \kappa_{rr} = 2.16 \times 10^{23} \beta P$ cm^2/s. For 1 GV particles in the outer heliosphere, this is 68% of the value of $\kappa/\beta \approx 3 \times 10^{23}$ cm^2/s used by Stone *et al.* (1996) to fit 1994 Voyager 1 and 2 ACR He and O observations. From this Table we also see

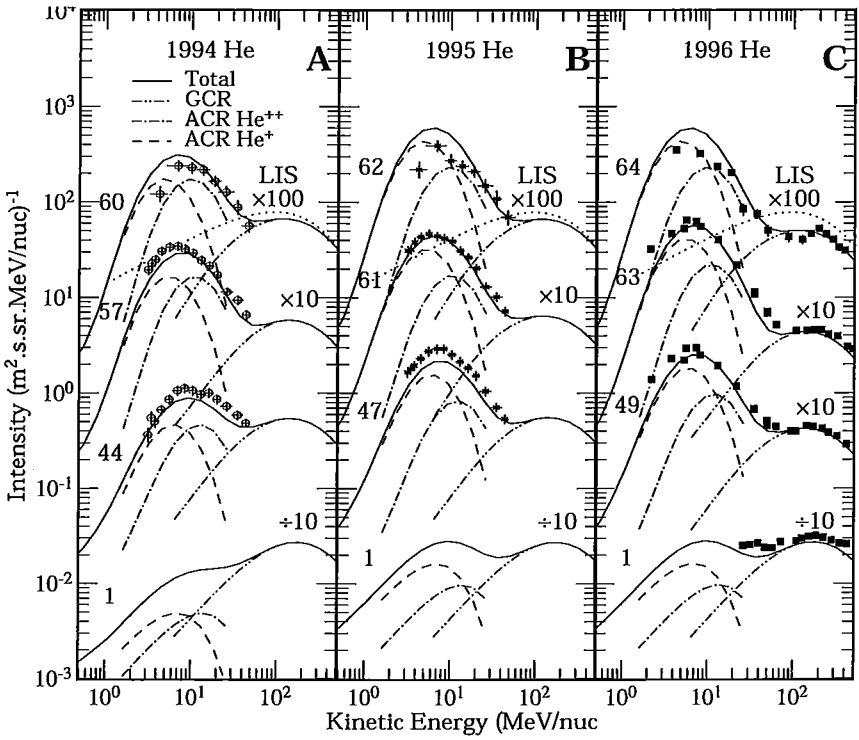

Figure 10. Model fits to the 1994/5/6 He observations in the same format as the observations presented in Figure 3.3, showing the modulated ACR He^{+}, He^{++} and GCR components at the spacecraft positions as indicated by the number to the left of each data set. The total modulated spectrum was calculated as the sum of the ACR and GCR components.

Table VI

Kinetic energies (MeV/nuc) at which the ACR He contribution to the total He intensity is largest. The percentage contribution at this energy is shown in brackets.

	IMP8	V2	V1	P10
1994	0.57 (46%)	4.6 (84%)	3.2 (92%)	3.2 (94%)
1995	0.57 (46%)	4.6 (94%)	3.2 (97%)	3.2 (98%)
1996	0.57 (53%)	4.6 (96%)	3.2 (98%)	3.2 (98%)

that the calculated source ratio of He^{+}/He^{++} increased from 1 in 1994 to 1.94 in 1995/1996.

Figure 10 shows that the fits to the observations are of similar quality to those for H, but with the calculated ACR radial gradients somewhat larger than observed.

Table VI shows the energies at which the maximum ACR He contribution occurs for the calculated spectra. For 1 AU these maxima of about 50% occur at 0.57 MeV/nuc, while they occur at $\approx$ 4.6 MeV/nuc for Voyager 2, and 3.2 MeV/nuc

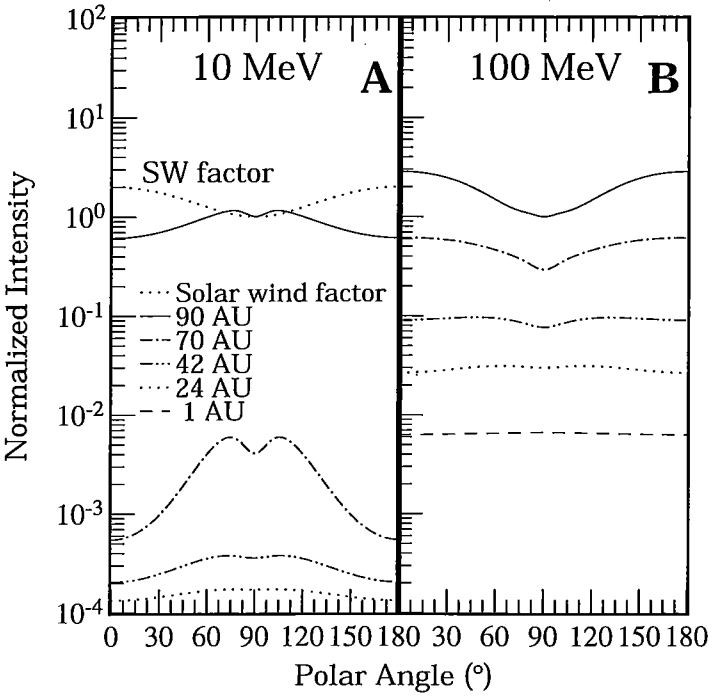

Figure 11. Latitudinal intensity profiles normalized to the intensity at the SWTS in the ecliptic plane. Due to the same modulation parameters for all three periods, these profiles are identical for 1994, 1995, and 1996 ACR H, and to those calculated for ACR He^{+} at 2.5 MeV/nuc and 25 MeV/nuc or 5 MeV/nuc and 55 MeV/nuc for ACR He^{++} for these three periods. Also shown is the assumed latitude variation of the solar wind (SW factor)

for Voyager 1 and Pioneer 10. As with H, the relative size of the ACR contribution increases towards the outer heliosphere, as well as from 1994 to 1996, with maximum calculated contributions of 98% at Voyager 1 and Pioneer 10 in 1996.

3.5. CONCLUSIONS

We have shown that it is possible to obtain reasonable quality, simultaneous, fits to the outer heliospheric ACR and GCR H and He observations for 1994, 1995 and 1996 using a full-drift modulation model. To achieve these fits, (a) the diffusion coefficients were taken to be the same for the three periods, (b) the ACR source function was smaller in 1994 than in 1995/96, (c) the local interstellar spectrum was taken to be a third of generally acceptable values, and (d) the diffusion coefficients for He were larger than the corresponding values for H. Point (c) is an indication that the diffusion coefficients used in these fits are too large for the GCR (higher rigidity) species. Point (d) is physically unacceptable because it implies different diffusion mean free paths for the two species.

It was found that a doubly charged ACR He^{++} component was required to explain the observed broad spectral peaks of ACR He. Furthermore, the ratio of ACR He^{+}/He^{++} was found to increase during the observation period (from 1994 to 1996). This result is, however, dependent on the rigidity dependence (βP) of the diffusion coefficients: a flatter (steeper) rigidity dependence will broaden (steepen) the modulated ACR peak widths.

These conclusions indicate that the model is not yet self-consistent and that the magnitude and rigidity dependence of the diffusion coefficients have to be explored further.